Locating the Ising conformal field theory via the ground-state energy on the fuzzy sphere

Kay Jörg Wiese

CNRS Laboratoire de Physique de l'Ecole Normale Supérieure, PSL Research University, Sorbonne Université, Université Paris Cité, 24 rue Lhomond, 75005 Paris, France

(Received 9 November 2025; revised 8 January 2026; accepted 12 January 2026; published 4 February 2026)

We locate the phase-transition line for the Ising model on the fuzzy sphere from a finite-size scaling analysis of its ground-state energy. Our strategy is to write the latter as $E_{\rm GS}(N_m)/N_m = E_0 + E_1/N_m + E_{3/2}/N_m^{3/2} + \cdots$ and to search for a minimum of $\chi := E_{3/2}/E_0$ as a function of the couplings. Conformal perturbation theory predicts that around a conformal field theory, $\chi = \chi_{\rm min} + \sum_i \lambda_i^2 N_m^{-\omega_i} + O(\lambda^3)$, where λ_i are the couplings associated with perturbations of operators with dimension Δ_i and $\omega_i = d - \Delta_i$. This procedure finds the critical curve of Zhu *et al.* [Phys. Rev. X **13**, 021009 (2023)] and its sweet spot with good precision. Varying two coupling constants allows us to extract the correction-to-scaling exponent ω associated with the two leading scalars ε and ε'. We find similar results when normalizing by the gap to the stress tensor T or the first parity-odd operator σ instead of E_0.

DOI: 10.1103/qzzt-86fn

I. INTRODUCTION

The fuzzy-sphere regularization is an exciting new tool [1] to access conformal field theories (CFTs) in dimension $d = 2 + 1$. The technique uses a 2-sphere inside of which s magnetic monopoles are placed. The lowest Landau level on this sphere is $N_m = 2s + 1$ times degenerate, each with $N_{\rm f}$ flavors ($N_{\rm f} = 2$ for the Ising model). Filling N_m of the $N_m \times N_{\rm f}$ states and adding interactions between the electrons allow one to engineer CFTs with a given symmetry. This approach was introduced in [1] to study the quantum two-dimensional Ising model, equivalent to the classical three-dimensional (3D) model. It has since been applied to other systems, including theories with global Sp(n) [2] or $O(3)$ [3] symmetry, Majorana fermions [4], a free scalar [5], Chern-Simons matter [6], the Potts model [7], and the Yang-Lee model [8–10]. The latter example is interesting as the theory is non-unitary, even though its spectrum is real; thus, it is not accessible via the numerical conformal bootstrap [11–15], which is the current gold standard for 3D CFTs.

While the method allows one to study phases as well as critical points, the latter are particularly interesting, especially when they correspond to a CFT. A crucial step is to identify the location of the critical point. The standard approach consists of choosing couplings which optimize the properties of the intended CFT, such as the integer spacing of descendants [1]. Doing so without assuming what one wants to show is critical. There have been interesting recent proposals [16,17] to construct the conformal generators on the fuzzy sphere, allowing one to check for the overlap of states expected to be descendants, with the constructed descendants being of expected primaries.

Here we locate the phase-transition line and sweet spot for the Ising model on the fuzzy sphere from a finite-size scaling analysis of the ground-state (GS) energy without using any information on higher excited states. Our procedure finds the critical curve of [1] with good precision and its sweet spot (the point of optimal conformality) as well.

II. SIZE DEPENDENCE OF THE GROUND STATE ENERGY

In dimension $d = 2$, the free energy per site of a classical CFT on a torus of circumference L is given by [18,19]

$$f(L) = f_\infty - \frac{\pi c}{6L^2} + O(L^{-3}). \tag{1}$$

Here f_∞ is the free energy per site in the limit of $L \to \infty$, and c is its central charge. This formula is valid at the critical point and can be used to locate it: First, one measures an effective central charge $c_{\rm eff}(g|L)$, where g is a microscopic coupling, via a fit to Eq. (1); then one demands that the theory is at a marginal point for $c_{\rm eff}(g|L)$ [20],

$$\partial_g c_{\rm eff}(g|L)\big|_{g=g^*} = 0 \Longrightarrow \lim_{L\to\infty} c_{\rm eff}(g^*|L) = c. \tag{2}$$

For a standard (real) CFT, a local maximum for $c_{\rm eff}(g|L)$ indicates a critical point, while a minimum indicates a critical phase. If the model at g^* is a CFT, then $c_{\rm eff}(g^*|L)$ converges for $L \to \infty$ to the central charge of the corresponding CFT.

The central charge has three properties: (1) It appears in the Virasoro algebra of conformal generators, (2) it governs finite-size corrections as in Eq. (1), and (3) it decreases along the renormalization group (RG) flow (Zamolodchikov's c theorem [21]). This motivates condition (2) for fixed points and explains why a critical point is a local maximum. The marginality condition (2) can also be used for complex CFTs and allowed the authors of [20] to locate the critical point of the five-state Potts model in $d = 2$, which has a complex second derivative and thus is neither the maximum nor minimum.

There is a generalization of Zamolodchikov's c theorem to $d = 4$, related to anomalies under Weyl rescaling [22,23], which gives the stress-energy tensor in the form [see Eq. (1.2) of [24]]

$$T^\mu_\mu = aE_4 - cW^2_{\mu\nu\rho\sigma}. \tag{3}$$

Here E_4 is the Euler density (which integrates to the Euler characteristic), and W is the Weyl tensor. It was first conjectured and checked to one-loop order by Cardy [25] and

later proven in [24] that a decays along RG trajectories (a theorem).

We now consider dimension $d = 3$. Reference [26] (Sec. 1) considers finite-size corrections for the free energy of a Euclidean field theory on a 3-sphere of radius R embedded into $\mathbb{R}^4$,

$$F = -\ln |Z_{S^3}| = \alpha_0 R^3 + \alpha_1 R + \mathcal{F}. \tag{4}$$

While α_0 and α_1 are nonuniversal, the last term, $\mathcal{F}$, is a number and may contain universal information. $\mathcal{F}$ was first obtained via holography [27] and in supersymmetric models [28] and only later was obtained for more general theories [29]. It took some time to find a proper definition which is universal and independent of the microscopic degrees of freedom [30,31]. Currently, the best approach to extract $\mathcal{F}$ is to study the entanglement spectrum [32]. References [31,32] proved that $\mathcal{F}$ so defined descends along the RG flow. Reference [33] succeeded in extracting $\mathcal{F}$ from the entanglement entropy on the fuzzy-sphere realization of the Ising model.

Now consider the free energy on $\mathbb{R}^3 \simeq \mathcal{S}_2 \times \mathbb{R}$, where the right-hand side is the geometry used in the fuzzy-sphere approach. To pass to the left, Euclidean time τ is mapped as $\tau \to e^{\tau}$, with $\tau \in [-\beta/2, \beta/2]$. For $\beta \gg R$, we expect the free energy to be

$$F = -\ln Z = \beta\Big[\alpha_0 R^2 + \alpha_1 + \frac{\alpha_{3/2}}{R} + \cdots\Big]. \tag{5}$$

The coefficient which may contain universal information is $\alpha_{3/2}$, as it is the only one without a scale. We can move to the quantum problem by taking $\beta \to \infty$,

$$E_{\rm GS}(R) = v_{\rm F}\Big[\alpha_0 R^2 + \alpha_1 + \frac{\alpha_{3/2}}{R} + \cdots\Big]. \tag{6}$$

Here $v_{\rm F}$ is an unknown Fermi velocity which, in general, depends on the microscopic couplings.

Let us explain why we did not include a term of order R in $E_{\rm GS}(R)$: The two leading terms in the vacuum energy allowed by geometry and necessitating counterterms (CTs) are

$$E_{\rm GS}^{\rm CT}(R) = \int \mathrm{d}^2x\,\sqrt{g}(\mu + \kappa\mathcal{R}), \tag{7}$$

where R is the radius of the sphere, $\mathrm{d}^2x\sqrt{g}$ is the invariant measure, μ is the coefficient of the vacuum-energy density ("cosmological constant"), and κ is the coefficient multiplying the curvature $\mathcal{R}$. According to the Gauss-Bonnet theorem, the latter integrates to $4\pi\chi$, where χ is the Euler characteristic; $\chi = 2$ for a sphere. As a result $E_{\rm GS}^{\rm CT}(R) = 4\pi R^2\mu + 8\pi\kappa$.

Using the identification that the area of the sphere grows with the number of electrons, or, more precisely [34],

$$N_m^2 = 1 + 4R^4, \tag{8}$$

we get for the GS energy per electron[1]

$$\frac{E_{\rm GS}(N_m)}{N_m} = E_0 + \frac{E_1}{N_m} + \frac{E_{3/2}}{N_m^{3/2}} + \cdots. \tag{9}$$

We recall that physical information is expected in $E_{3/2}$. This is in line with the observation that the gap of any excited state has the same scaling in N_m as $E_{3/2}$ (for the stress-energy gap $E_T - E_{\rm GS}$ see the discussion and Fig. 9 below); thus, if one looks for a coefficient of the GS energy which is universal, one again concludes that the only viable candidate is $E_{3/2}$.

At this point it is interesting to recall a standard tool in data analysis, the Binder cumulant, also known as kurtosis (the ratio of the fourth moment divided by the square of the second moment). In the vicinity of a phase transition, it takes the form

$$\mathcal{B}(\{\lambda_i\}|R) = \mathcal{B}_0 + p(\{\lambda_i R^{-\omega_i}\}), \quad \omega_i = \Delta_i - d, \tag{10}$$

where $\mathcal{B}_0$ is a number and p is a function in the couplings λ_i associated with perturbations by operators of dimension Δ_i.[2] We postulate that $E_{3/2}$ can play a role similar to the Binder cumulant in locating the point where finite-size corrections are minimized.

Now consider the behavior close to a CFT. There the action takes the form

$$\mathcal{S} = \mathcal{S}^{\rm CFT} + \sum_i \lambda_i \int_x \mathcal{X}_i(x), \tag{11}$$

where $\mathcal{X}_i(x)$ are primaries. Schematically, the free energy in statistical field theory is [35]

$$F = -\ln Z = F_0^{\rm CFT} + \sum_i \lambda_i \int_x \langle \mathcal{X}_i(x)\rangle_{\rm CFT} - \frac{1}{2}\sum_{i,j}\lambda_i\lambda_j \int_{x_1}\int_{x_2} \langle \mathcal{X}_i(x_1)\mathcal{X}_j(x_2)\rangle^{\rm c}_{\rm CFT} + \cdots. \tag{12}$$

As the vacuum expectation of primaries vanishes, the linear terms are absent. At second order, only the term with $i = j$ survives. The result is

$$F = F_0^{\rm CFT} - \sum_i (\lambda_i R^{d-\Delta_i})^2. \tag{13}$$

We have not specified our domain of integration and absorbed possible geometrical factors into λ_i. Equation (13) has a factor of R^{2d} from the integration measure and a factor of $R^{-2\Delta_i}$ from the two-point function $\langle \mathcal{X}_i(0)\mathcal{X}_i(R)\rangle = R^{-2\Delta_i}$. An equivalent procedure can be performed in the quantum-formulation [36,37] which uses the sphere as geometry.[3] We conclude that

$$E_{3/2} = E_{3/2}^{\rm CFT} - \sum_i (\lambda_i R^{d-\Delta_i})^2 + O(\lambda_i^3). \tag{14}$$

A cubic term is expected because there are nonvanishing three-point functions. Equation (14) is of the form postulated in Eq. (10). In order to eliminate the Fermi velocity $v_{\rm F}$ in

[1] The GS energy given by FuzzifiED is indeed $\sim N_m$.

[2] When a perturbative expansion in λ_i exists, p is a polynomial.

[3] In this formulation, the integration measure gives R^{2d-2}. The seemingly missing factor of R^2 is provided by the denominator $E_i - E_{\rm GS} \sim R$, correcting an energy $\sim R$. The quantum version, with its well-defined geometry, is appropriate for evaluating the geometrical prefactors.

Eq. (6), below we shall analyze[4]

$$\chi := \frac{E_{3/2}}{E_0}. \tag{15}$$

(Alternative normalizations are discussed in Sec. III F.) Since in our problem E_0 is negative, a CFT implies a minimum of χ. Around this minimum, we expect

$$\chi = \chi_{\min} + \sum_i \frac{\lambda_i^2}{N_m^{\omega_i}}, \quad \omega_i = \Delta_i - d. \tag{16}$$

As we show below, this procedure finds the critical curve and the sweet spot of [1] with good precision. The standard algorithm to locate a CFT is to search for a spectrum with integer-valued spacing for descendants of primary operators, as dictated by CFT [1], or to explicitly check for conformal symmetry [16,17]. Our procedure is an alternative. Its sole ingredient is the GS energy. Its advantages are that it is simple to implement and computationally fast.

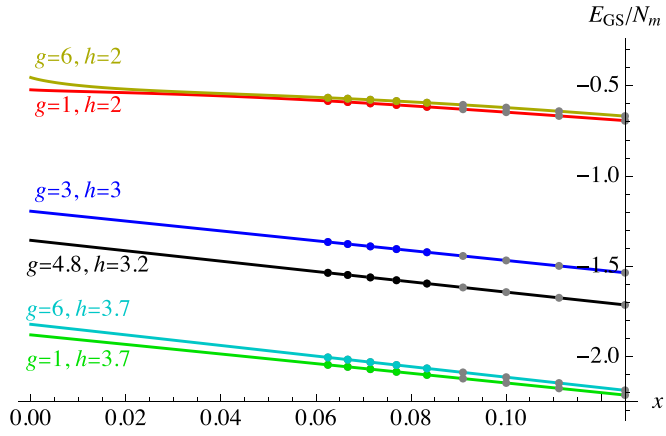

FIG. 1. $E_{GS}(x)$ for various values of h and g for $o = 4$, using $x^{i/2}$ as a basis, $\{1, x, x^{3/2}, x^2, x^{5/2}\}$, $N_m^{\max} = 16$. Gray dots are not used for the fit but are in agreement with it.

III. FINITE-SIZE SCALING ANALYSIS OF THE GROUND-STATE ENERGY

A. Model

We use the Ising model defined in the seminal work [1]. It consists of a 2-sphere with s magnetic monopoles at its center, onto which are placed $N_m = 2s + 1$ fermions, each with two internal degrees of freedom (up and down spins). Without interactions, the spectrum is flat. One then introduces a repulsive interaction upon contact between electrons pointing in the z direction of strength $g = V_0$ and a "kinetic" term (coupling to the gradient of the density interactions) of strength $V_1 = 1$ in the same direction. Finally, a transverse magnetic field of strength h drives the phase transition, similar to what happens in the one-dimensional spin chain.

For the implementation, see Appendix A.

B. Dependence of the GS energy on system size

We developed the ansatz (9) for the GS energy. In the rest of this work, we use this ansatz with two additional subleading terms,

$$\frac{E_{GS}(x|h,g)}{N_m} = E_0(h,g) + E_1(h,g)x + E_{3/2}(h,g)x^{\frac{3}{2}} + E_2(h,g)x^2 + E_{5/2}(h,g)x^{\frac{5}{2}} + \cdots, \tag{17}$$

$$x := \frac{1}{N_m}. \tag{18}$$

Let us check this against exact diagonalization. Figure 1 shows that the GS has both a constant E_0 and a strong linear component E_1. We tried adding a term of order $\sqrt{x}$ and found that its coefficient is either absent or very small. Out of curiosity, we also tried an ansatz with integer coefficients. We found that information about the critical line can be extracted but seems to sit in higher derivatives, which we do not find convincing (see Appendix B). We also played with different orders of the truncation. We trust our analysis when higher-order coefficients are small. With its almost straight behavior, Fig. 1 [which uses Eq. (17)] suggests that the leading term in the expansion is indeed of order x and not $\sqrt{x}$ or that at least the coefficient $\sim\sqrt{x}$ is very small, and we discard it. Adding terms beyond $E_{3/2}$ seems helpful (see Appendix B).

We now look at the GS energy extrapolated to $x = 0$. As Fig. 2 attests, this is rather featureless. A crucial problem with quantum-mechanical approaches is that all energy levels are multiplied by an unknown Fermi velocity v_F [see Eq. (6)]. In the fuzzy-sphere approach, this is usually fixed by demanding that the stress-energy tensor have dimension $d = 3$. An alternative is to prescribe the energy of the first excited state σ, which suffers less from finite-size corrections close to the Ising CFT [37]. Our goal here is to extract the location of the CFT solely from the GS energy. To eliminate the unknown Fermi velocity, we consider finite-size corrections normalized

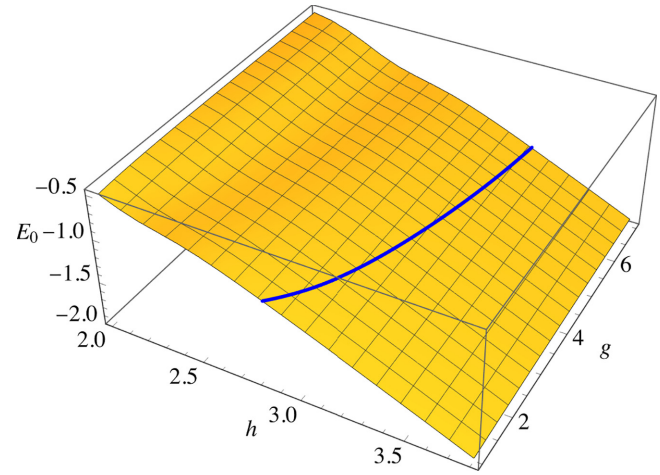

FIG. 2. $E_0 = E_{GS}(0|h,g)$ for $o = 4$, $N_m^{\max} = 17$; this plot changes little between $N_m^{\max} = 13$ and $N_m^{\max} = 17$. The critical line is in blue.

[4]If there are perturbative corrections to E_0, we expect them to take the same form as in Eq. (14), so that the argument remains valid for the ratio.

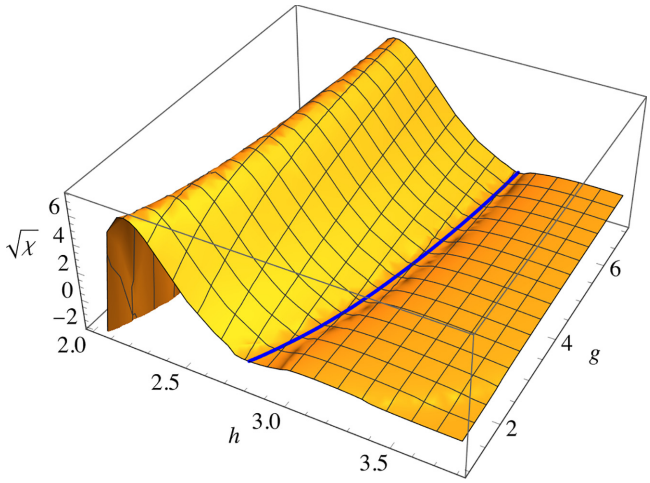

FIG. 3. χ for $N_m^{\max} = 17$. The critical line is in blue. To make the minimum visible, we plot the signed root ($\sqrt{\chi} := \mathrm{sgn}(\chi)\sqrt{|\chi|}$). To enhance the resolution of the plot, the interpolation outlined in Eq. (20) and Fig. 5 was used. Compare to Fig. 4.

by the extrapolated GS energy, i.e.,

$$\chi(h, g) := \frac{E_{3/2}(h, g)}{E_0(h, g)}, \tag{19}$$

where the coefficients are those of Eq. (17). Alternative normalizations are discussed in Sec. III F.

C. Implementation

Our ED data are such that we can use $N_m = 8$ to 17, i.e., a maximal N_m per fit of $N_m^{\max} = 12$ to 17. Large sizes are possible since we need only the GS energy. For the order of approximation, we tried $o = 2$, 3, 4, 5, and 6 (o counts the number of terms beyond the constant E_0). Larger orders o are not necessarily better, as numerical artifacts are amplified in ways possibly not detectable. Common sense and experience lead us to consider $o = 4$ optimal, i.e., the form given in Eq. (17).

We now evaluate χ: Following [1], we plot h on the horizontal axis and g on the vertical axis. We first show a 3D plot in Fig. 3 and then a heat plot in Fig. 4. On the latter, the critical line of [1] is given in white (partially hidden under blue dots), with a white shamrock marking their *sweet spot* (the best agreement with the Ising CFT). The dark blue dots in Fig. 4 mark the valley floor, defined as follows: Look at the Hessian $H_{ij} := \partial_i \partial_j \chi(h, g)$, where $i, j \in \{h, g\}$. Since H_{ij} is symmetric, it has two eigenvalues, the curvatures, and two eigenvectors, which are orthogonal. We take the eigenvector in the direction of the larger curvature and require that the slope in this direction vanishes.[5]

This is a highly nonlinear operation on the numerical data generated on a grid with step size $\delta h = 1/20$ and $\delta g = 1/5$,

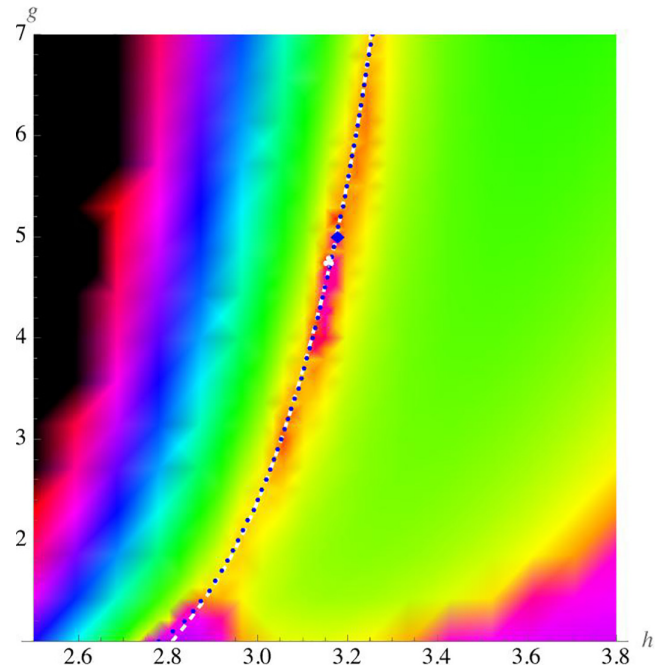

FIG. 4. Heat map of $\chi(h, g)$ given in Eq. (15) for $o = 4$ and $N_m^{\max} = 17$. Compare to Fig. 3. The white dashed line is the critical line of [1], with a white shamrock marking its sweet spot (best agreement with a CFT). This line was extracted from Fig. 2 of [1]; the sweet spot of [1] is $h = 3.16$ and $g = 4.75$. Dark blue dots show the minimum of the valley of $\chi(h, g)$. The blue diamond marks the global minimum of $\chi(h, g)$.

for which we need a smooth interpolation. This is obtained by fitting a polynomial of maximal degree 4 (15 coefficients) to the 6×6 neighbors, weighted by

$$\rho(h, g) := \exp\left(-\alpha\left[\frac{(h_i - h)^2}{\delta h^2} + \frac{(g_i - g)^2}{\delta g^2}\right]\right), \tag{20}$$

where $\alpha = 0.6$ is a phenomenological parameter. An example of the weights is given in Fig. 5. Compared to lattice-based approaches which are discontinuous when a new interpolation

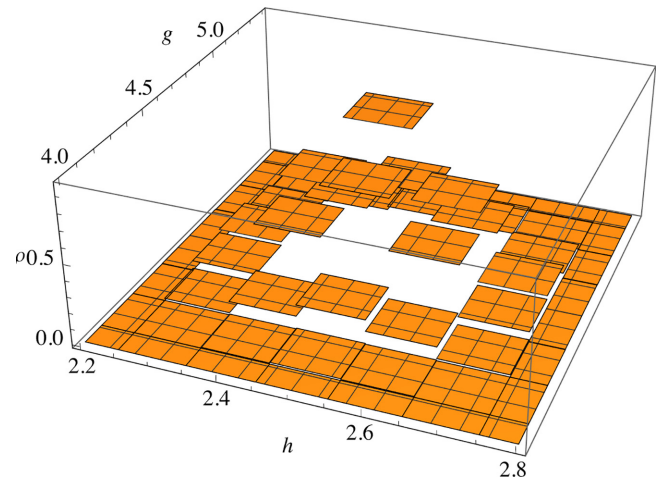

FIG. 5. The weights $\rho(h, g)$ defined in Eq. (20) for $h = 2.5$ and $g = 4.75$ (off grid).

[5]This definition uses the metric of the coordinates h and g. It is not invariant under reparametrization, e.g., $\{h, g\} \to \{h, g + h\}$. The result is rather similar if we look at a vanishing slope in the h direction. Not knowing the metric will haunt us later (see Sec. III E).

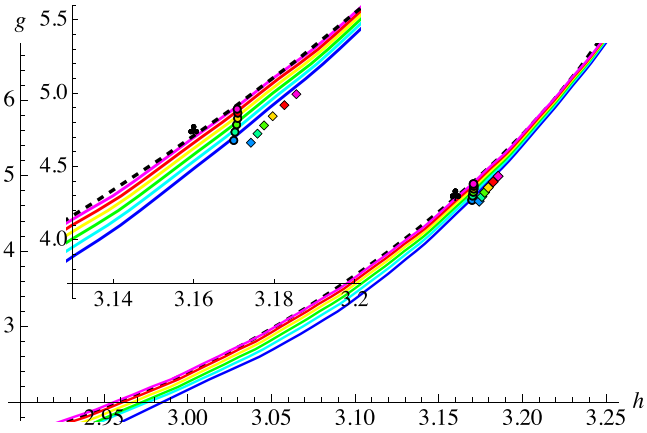

FIG. 6. Main plot: Dependence on $N_m^{\max}$ of the critical curve and sweet spot (dots) for a grid with $\delta g = 0.2$ and $\delta h = 0.05$, ranging from $N_m^{\max} = 12$ (blue) to $N_m^{\max} = 13$ (cyan) to $N_m^{\max} = 17$ (magenta); diamonds mark the minimum on a microgrid with discretization $\delta g = 0.05$ and $\delta h = 0.01$ (transition line not shown). The inset shows a blowup around the sweet spot. Deviations are indicative of errors due to the finite grid size. The black dashed line shows the critical line extracted from [1]; a black shamrock marks its sweet spot.

point enters, our procedure is very smooth. If the data turn out to be noisy, one can decrease α to effectively include more points in the fit. The number of neighbors is chosen such that additional points have vanishing weight.

D. Results for the location of the critical point

As Fig. 4 attests, we can locate the phase-transition line of Ref. [1], which corresponds to the white dashed line. Our valley of $\chi(h, g)$ is marked by blue dots. On this phase-transition line the best agreement with the Ising CFT is achieved at the position of the white shamrock [1], while the nearby global minimum of $\chi(h, g)$ is marked by a blue diamond. For a CFT, the latter minimum satisfies

$$\partial_h \chi(h, g) = \partial_g \chi(h, g) = 0. \tag{21}$$

How this minimum depends on the system size is shown in Fig. 6. There is a small systematic upwards drift on the minima obtained via interpolation (dots). We repeated the analysis on a much finer grid ("microgrid") with $\delta g = 0.05$ and $\delta h = 0.01$ around the sweet spot, obtaining comparable results (see the diamonds in Fig. 6 and the table in Fig. 7). The reader may worry about the small drift visible in Fig. 6 and

$N_m^{\max}$	h	g	$\chi_{\min}$	$\chi''_{\max}$	$\chi''_{\min}$
12	3.17422	4.66314	0.0056442	10.97	0.01907
13	3.17587	4.72479	0.0054353	12.86	0.01188
14	3.17750	4.78087	0.0050100	14.88	0.00780
15	3.17965	4.84383	0.0045505	17.01	0.00599
16	3.18256	4.91919	0.0041134	19.27	0.00496
17	3.18553	4.99396	0.0037134	21.64	0.00441

FIG. 7. Values for the minimum of χ, its location, and the two eigenvalues of $\chi'' = \partial_i \partial_j \chi$, with $i, j = h, g$ for different $N_m^{\max}$, obtained on a grid with $\delta g = 0.05$ and $\delta h = 0.01$.

agreement with the results of [1]. In the latter work, the critical line of Fig. 2 was obtained for fixed $V_0 = g$ by scanning over h and reporting the point [see [1], Fig. 3(a)] where $\langle M^2 \rangle / N_m^{2-\Delta_\varepsilon}$ and $\Delta_\varepsilon = 0.518148$ (from the numerical conformal bootstrap) cross for different N_m. On this critical line, the sweet spot (the point of optimal conformality) was obtained by minimizing a cost function [1], resulting in [38]

$$g_c = 4.75 \pm 0.01, \quad h_c = 3.16 \pm 0.01. \tag{22}$$

The drift observed in Fig. 6 is below the resolution of the coarse grid and comparable to that of the fine grid. The result in Eq. (22) seems more precise, but we did not use the value of Δ_ε. In contrast, our result seems to be more precise than what one can obtain from the Binder cumulant [see [1], Fig. 3(b)]. One may also make a comparison to Fig. 5 of [16]; apart from "islands of confidence," the authors reported where conformal perturbation theory has vanishing couplings (compare to Fig. 4 for $N_m = 12$ and the blue data in Fig. 6):

$$V_0 \equiv g = 4.825, \quad h = 3.158 \quad (N_m = 12). \tag{23}$$

In summary, all results seem to be consistent, even if there is a small systematic drift towards larger h and g with increasing N_m. A definite answer would require evaluating the spectrum at larger system sizes than used, e.g., in [16] [see Eq. (23)].

E. Curvature scaling

Equation (16) states how χ behaves close to its minimum. Since our numerical data are obtained with two parameters, $\{h, g\}$, we should see an approximation involving the two leading parity-even scalars ε and ε':

$$\chi \simeq \chi_{\min} + \frac{\lambda_1^2}{N_m^{\omega_1}} + \frac{\lambda_2^2}{N_m^{\omega_2}}, \tag{24}$$

$$\begin{pmatrix} \lambda_1 \\ \lambda_2 \end{pmatrix} = \mathbb{M} \begin{pmatrix} h - h_c \\ g - g_c \end{pmatrix}. \tag{25}$$

The matrix $\mathbb{M}$ has four parameters. Two can be used for rescaling λ_1 and λ_2; since this only shifts the curves in Fig. 8 vertically, we discard it. The next parameter is for a rotation. Independent of N_m, we find a rotation by -0.046 rad ($-2.7°$). As a result, $h - h_c$ strongly aligns with λ_1. In Fig. 8 we show how the largest and smallest eigenvalues of $\chi'' := \partial_i \partial_j \chi$, with $i, j = h, g$ (see Fig. 7), scale with N_m. This allows us to extract $\omega_1 \approx -1.9$ and $\omega_2 \approx 2.7$ from the last two data points. We plot the successive slopes in the middle panel of Fig. 8. For ω_1 it allows us to extrapolate $N_m \to \infty$, resulting in

$$\omega_1 \approx -1.60, \quad \omega_\varepsilon = \Delta_\varepsilon - 3 = -1.58738. \tag{26}$$

This is close to the numerical bootstrap result [12] for ε.

It is more delicate to extract ω_2, as the decreasing slope in the left plot in Fig. 8 (shown in the middle plot) asserts. We still have one parameter left in $\mathbb{M}$: It corresponds to an angle different from 90° between the microscopic coupling constants. To exploit this, a simple procedure is to write χ to second order as

$$\tilde{\chi} = \chi''_{\max} \frac{\lambda_1^2}{2} + \chi''_{\min} \frac{\lambda_2^2 + \alpha \lambda_1 \lambda_2}{2} \tag{27}$$

and redo the scaling analysis of the data in Fig. 7 with the eigenvalues of $\partial_i \partial_j \tilde{\chi}$, optimizing α such that the last three

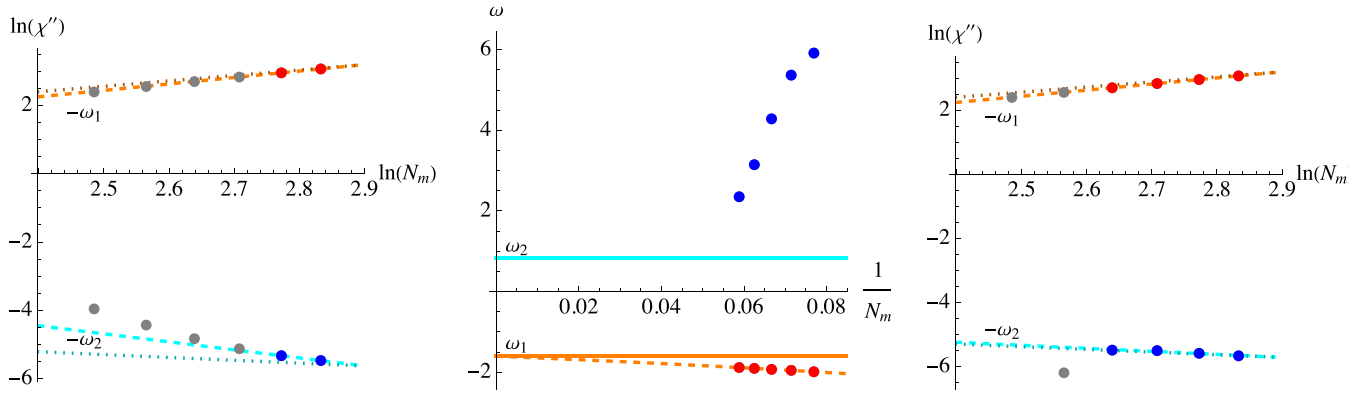

FIG. 8. Left: Scaling of the two eigenvalues of $\partial_i\partial_j\chi$ (with $i = h, g$) with respect to N_m. The dashed lines are fits with $\omega_1 \approx -1.9$ and $\omega_2 \approx 2.7$; the dotted lines show the expected slopes. Gray dots are not included in the fit. Middle: Extrapolation of ω_1 and ω_2 to $N_m = \infty$ (using a quadratic polynomial for ω_1). We find $\omega_1 \approx -1.60$ and $\omega_2 \approx 1$, which should be compared to $\omega_\varepsilon = \Delta_\varepsilon - 3 = -1.58738$ and $\omega_{\varepsilon'} = \Delta_{\varepsilon'} - 3 = 0.82968$ (solid lines) [12]. Right: Using a skew transformation to align the last three points for ω_2 (see text) gives ω_1 as before and $\omega_2 = 0.94$, which is now close to the expected results.

points for ω_2 lie on a straight line (see the right plot in Fig. 8). With the optimal $\alpha = 59.868$ we find the last four points to align, which allows us to extract

$$\omega_2 \approx 0.94, \quad \omega_{\varepsilon'} = \Delta_{\varepsilon'} - 3 = 0.82968. \tag{28}$$

This is now close to the prediction [12] from the numerical bootstrap for ε'. As we have exhausted our free parameters, we cannot go further.

F. Alternative normalizations

The alert reader will object that E_0 is not universal.[6] We propose two ways out of this dilemma which require calculating one more eigenvalue, either E_T, the subleading contribution in the GS sector corresponding to the stress-energy tensor, or E_σ, the lowest-lying parity-odd state.

[6]Our procedure continues to work as long as $E_0(h, g) - E_0(h_c, g_c)$ has an expansion of the form (14).

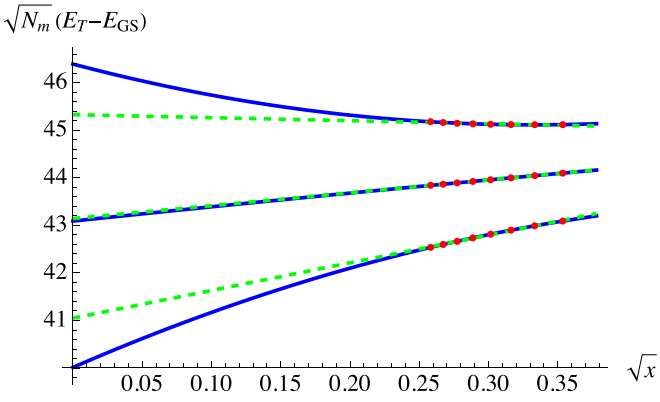

FIG. 9. The rescaled stress-energy tensor gap $\sqrt{N_m}(E_T - E_{GS})$ ($\ell = 2$, $P = Z = 1$) close to the sweet spot: $g = 4.8$ and $h = 3.1$ (bottom), $h = 3.2$ (middle), and $h = 3.3$ (top). Fits to $\{1, \sqrt{x}, x\}$ (blue) are compared to a linear fit (dashed green line). Interestingly, the curvature changes sign at the transition.

Let us first consider E_T. In Fig. 9 we show how weakly $E_T - E_{GS}$ depends on x. We found it appropriate to fit to $\{1, \sqrt{x}, x\}$. Interestingly, the curvature in $\sqrt{x}$ changes sign at the transition; one should explore this further. Figure 10 shows the resulting extrapolated value of the stress-energy gap as a function of h and g. This allows us to define

$$\chi_T := \frac{E_{3/2}}{\sqrt{N_m}(E_T - E_{GS})}. \tag{29}$$

A plot of this function is shown in Fig. 11, which should be compared to Fig. 3.

The second alternative is to normalize by the gap of the first parity-odd operator σ,

$$\chi_\sigma := \frac{E_{3/2}}{\sqrt{N_m}(E_\sigma - E_{GS})}. \tag{30}$$

While the σ gap is rather insensitive to perturbations close to the Ising CFT [37], it depends strongly on h, as Fig. 12 attests. Trying to extrapolate to $N_m = \infty$ even with a linear fit in $\sqrt{x}$ and two consecutive system sizes leads to a nonsensical negative gap. For this reason, we use only one system size for

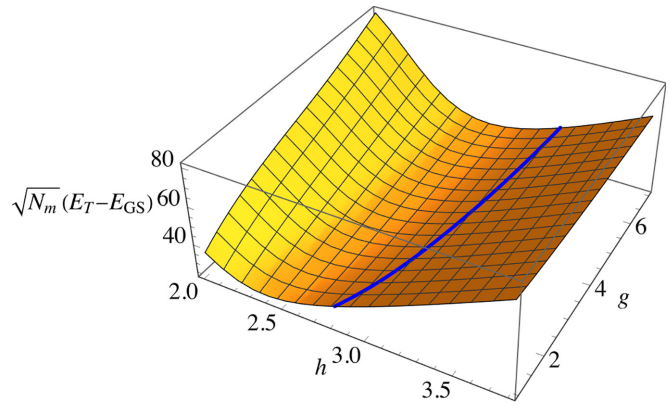

FIG. 10. The stress-energy tensor gap ($\ell = 2$, $P = Z = 1$) multiplied by $\sqrt{N_m}$ and extrapolated to $x = 0$, fit to $\{1, x^{1/2}, x\}$ and $N_m^{max} = 15$.

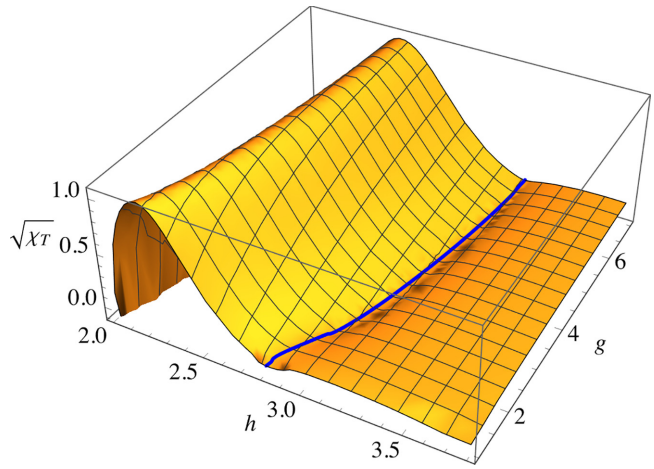

FIG. 11. χ_T for $N_m^{\max} = 15$. The critical line is shown in blue. We use the same approach as in Fig. 3 for χ.

the normalization in Eq. (30). The result is shown in Fig. 13, which should be compared to Figs. 3 and 11.

We now use χ, χ_T, and χ_σ at $N_m^{\max} = 15$ and repeat the analysis for the critical line and sweet spot. Figure 14 shows this comparison for a slightly coarser grid with $\delta g = 0.2$ and $\delta h = 0.1$. The resulting phase-transition lines lie close together, as do their sweet spots; deviations are well below the resolution of the computing grid. Our conclusion is that χ, χ_T, and χ_σ give comparable results.

G. Universality and $\mathcal{F}$ function

The function $\mathcal{F}$ in Eq. (4) is universal, and recently, values for it were reported:

$$\begin{aligned} \mathcal{F}_{\text{free theory}} &= \frac{\ln(2)}{8} - \frac{3\zeta(3)}{16\pi^2} \simeq 0.0638071, \\ \mathcal{F}_{\text{Ising}}^{\text{fuzzy}} &= 0.0612(5) \quad \text{(fuzzy sphere)}, \\ \mathcal{F}_{\text{Ising}}^{4-\varepsilon} &= 0.0610 \quad (4-\epsilon) \end{aligned} \tag{31}$$

(see [29,33,39], respectively). Can $\mathcal{F}$ be accessed in our approach? An obvious guess is to take $E_{3/2}$ in units of the stress-energy tensor,[7]

$$\mathcal{F} \stackrel{?}{=} 3\chi_T. \tag{32}$$

At size $N_m = 15$, we find at the sweet spot

$$3\chi_T \approx 0.00013 \quad \text{at } h = 3.16, \quad g = 4.51. \tag{33}$$

This value is much smaller than $\mathcal{F}$ reported in Eq. (31). It seems that in our approach χ may even vanish, as we test in Fig. 15: We evaluated χ at the sweet spot of [1] using density matrix renormalization group (DMRG) results for larger systems (the last point at $N_m = 23$ may not have converged). By plotting both χ and $\chi\sqrt{N_m}$ we see that this is consistent with $\chi = 0$ at the sweet spot. So either much larger system

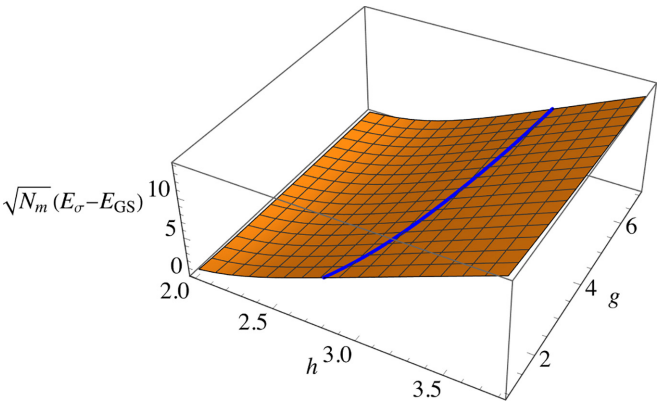

FIG. 12. $\sqrt{N_m}(E_\sigma - E_{\text{GS}})$ for $N_m = 15$. Note that the gap vanishes for small h which is in the non-critical ferromagnetic phase.

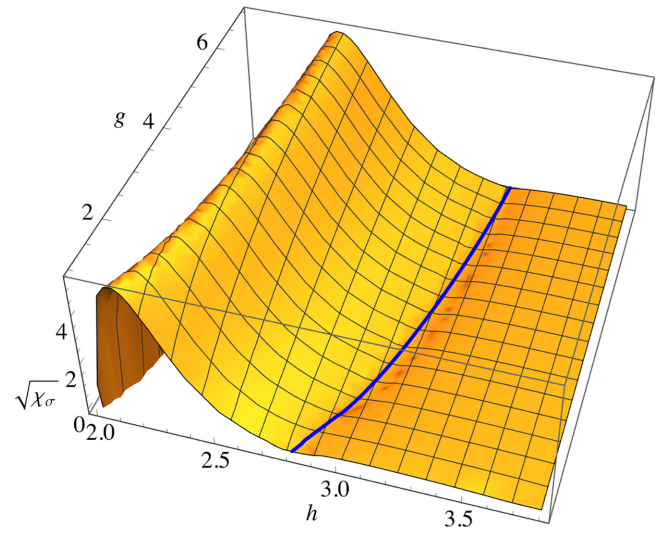

FIG. 13. χ_σ for $N_m^{\max} = 15$. The critical line is shown in blue. We use the same approach as in Fig. 3 for χ, plotting the signed root $\sqrt{\chi_\sigma}$.

[7]The number $d = 3$ is the dimension of the stress-energy tensor.

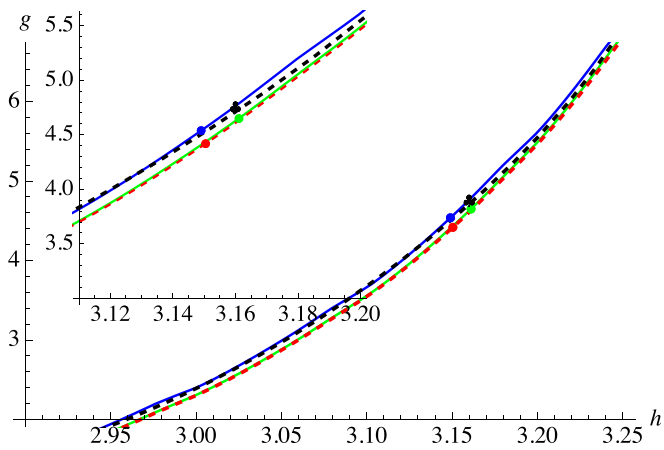

FIG. 14. The same as Fig. 6, with different denominators at size $N_m^{\max} = 15$: χ (green line), χ_T (red dashed line) and χ_σ (blue line). The black dashed line shows the critical line of [1], with a black shamrock marking its sweet spot.

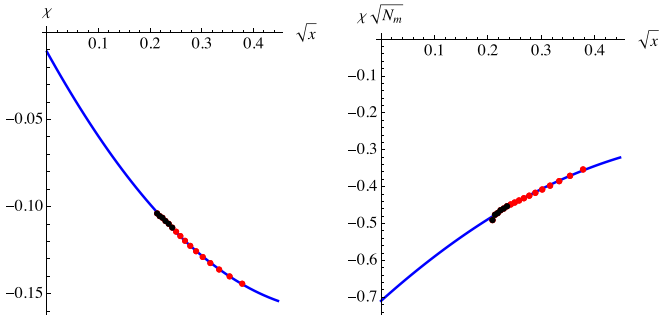

FIG. 15. Left: χ as a function of $\sqrt{x}$ for N_m ranging from $N_m = 6$ to $N_m = 23$ at the sweet spot of [1], namely, $g = 4.75$ and $h = 3.16$. The black points are obtained via DMFT, and small numerical errors increase with the differences we take. (This is apparent in the last data point.) Right: The extrapolated value is so small that it is consistent with a different scaling; namely, $\chi\sqrt{N_m}$ converges for $N_m \to \infty$. All fits are quadratic polynomials in $\sqrt{x}$.

sizes are needed to extract $\mathcal{F}$, or χ_T has no connection to $\mathcal{F}$ and vanishes at the transition. This may be expected, given that a quantum system on the fuzzy sphere is equivalent to $S_2 \times \mathbb{R} = \mathbb{R}^3$, and the latter should not have an anomaly.

IV. CONCLUSION

We have shown how the phase-transition line on the fuzzy sphere, and the sweet spot of optimal conformality can be obtained from a finite-size analysis of the ground-state energy. This was achieved by analyzing the term of relative order $N_m^{-3/2}$ in the ground-state energy, divided by the leading term, as a function of N_m. It yields the phase-transition line of [1] and their sweet spot with good precision. While small system sizes such as $N_m = 12$ already allow us to locate the phase transition, the precision increases for larger N_m. A non-negligible advantage of our approach is that it requires us to find only the ground-state energy instead of the full spectrum, which is computationally fast: We need about 10 min for $N_m = 17$ on eight cores.

An alternative which does not normalize via the ground-state energy is to use either the stress-energy gap or the gap of σ. Both procedures take a universal normalization and give comparable results but are computationally slightly more costly.

We hope this procedure may prove useful for locating the critical point in models such as the three-state Potts model in dimension $d = 3$, where the transition for real couplings is first order [7,40,41]. Suppose we know an approximate location of the minimum in the real plane. We can then approximate $\chi(h, g)$ by a polynomial around this point and search for solutions of Eq. (21) in the complex plane, near the approximate minimum.

ACKNOWLEDGMENTS

The author thanks A. Nahum, J. Rong, and S. Rychkov for valuable discussions; Y.-C. He, J. Jacobsen, A. Nahum, Z. Zhou, and W. Zhu for feedback on the draft; and W. Zhu for providing the error bars in Eq. (22).

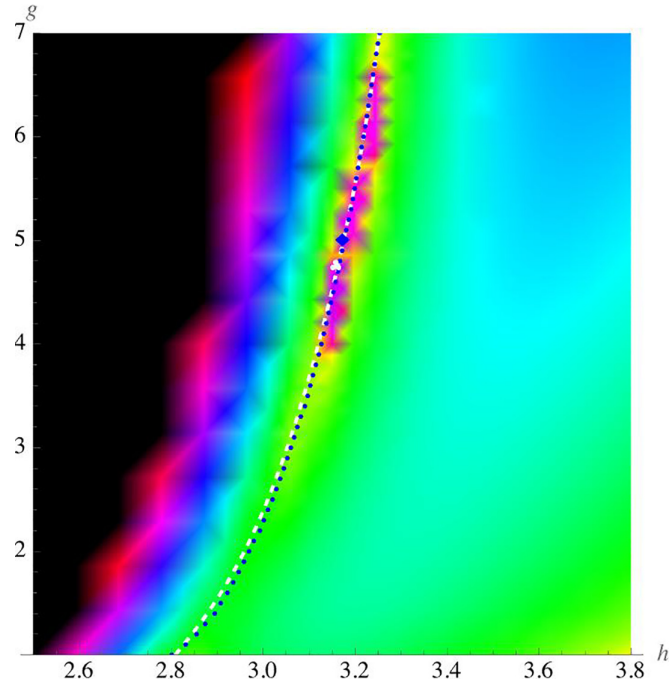

FIG. 16. The same as Fig. 4 at $N_m^{\max} = 17$ when using a polynomial in x of degree 4 for the fit and analyzing $-E_3/E_0$.

DATA AVAILABILITY

The data that support the findings of this article are not publicly available upon publication because it is not technically feasible and/or the cost of preparing, depositing, and hosting the data would be prohibitive within the terms of this research project. The data are available from the authors upon reasonable request.

APPENDIX A: FuzzifiED

We use the package FuzzifiED [42]. It provides a compact and efficient implementation to obtain the spectrum of a user-defined model on the fuzzy sphere using both exact diagonalization and DMRG. The package is described in detail in [34]. The program we used is an adaptation of ising_spectrum.jl, wrapped inside a *Mathematica* loop. To avoid numerical errors, we eliminated the rounding, i.e., the instruction "round.([enrg[i], l2_val[i], P, Z], digits = 6)." For system sizes $N_m \geqslant 16$ we restrict the evaluation to the GS energy, leading to a considerable speedup. (We can do $N_m = 17$ in about 10 min on eight cores, using a machine from 2013.)

APPENDIX B: DIFFERENT EXTRAPOLATION SCHEMES

Since the term $E_{3/2}$ seemingly vanishes at the transition, we can try to extract the phase-transition line from a fit to a polynomial in x. Reasonable agreement was achieved by considering a term of order x^4, as shown in Fig. 16. It finds the phase-transition line, as well as the sweet spot, albeit with less precision. While we do not know whether this somehow arbitrary procedure may have a use, it indicates that the proposed approach is rather robust.

A final note of caution. When using Eq. (17), it is important to not terminate the expansion at $E_{3/2}$ and to keep the two following coefficients: E_2 and $E_{5/2}$. Dropping $E_{5/2}$ still allows one to see the phase transition, albeit only at large N_m and with less precision; the sweet spot moves to $h = 3.2$ and $g = 5.3$. Dropping both terms gives a nonsensical result.

[1] W. Zhu, C. Han, E. Huffman, J. S. Hofmann, and Y.-C. He, Uncovering conformal symmetry in the 3D Ising transition: State-operator correspondence from a quantum fuzzy sphere regularization, Phys. Rev. X **13**, 021009 (2023).

[2] Z. Zhou and Y.-C. He, A new series of 3D CFTs with Sp(n) global symmetry on fuzzy sphere, Phys. Rev. Lett. **135**, 026504 (2025).

[3] A. Dey, L. Herviou, C. Mudry, and A. M. Läuchli, Conformal data for the $O(3)$ Wilson-Fisher CFT from fuzzy sphere realization of quantum rotor model, arXiv:2510.09755.

[4] Z. Zhou, D. Gaiotto, and Y.-C. He, Free Majorana fermion meets gauged Ising conformal field theory on the fuzzy sphere, arXiv:2509.08038.

[5] Y.-C. He, Free real scalar CFT on fuzzy sphere: Spectrum, algebra and wavefunction ansatz, arXiv:2506.14904.

[6] Z. Zhou, C. Wang, and Y.-C. He, Chern-Simons-matter conformal field theory on fuzzy sphere: Confinement transition of Kalmeyer-Laughlin chiral spin liquid, arXiv:2507.19580.

[7] S. Yang, Y.-G. Yue, Y. Tang, C. Han, W. Zhu, and Y. Chen, Microscopic study of 3D Potts phase transition via fuzzy sphere regularization, Phys. Rev. B **112**, 024436 (2025).

[8] R. Fan, J. Dong, and A. Vishwanath, Simulating the non-unitary Yang-Lee conformal field theory on the fuzzy sphere, arXiv:2505.06342.

[9] E. A. Cruz, I. R. Klebanov, G. Tarnopolsky, and Y. Xin, Yang-Lee quantum criticality in various dimensions, arXiv:2505.06369.

[10] J. E. Miro and O. Delouche, Flowing from the Ising model on the fuzzy sphere to the 3D Lee-Yang CFT, J. High Energy Phys. 10 (2025) 037.

[11] M. Reehorst, S. Rychkov, D. Simmons-Duffin, B. Sirois, N. Su, and B. van Rees, Navigator function for the conformal bootstrap, SciPost Phys. **11**, 072 (2021).

[12] D. Poland, S. Rychkov, and A. Vichi, The conformal bootstrap: Theory, numerical techniques, and applications, Rev. Mod. Phys. **91**, 015002 (2019).

[13] S. El-Showk, M. F. Paulos, D. Poland, S. Rychkov, D. Simmons-Duffin, and A. Vichi, Solving the 3D Ising model with the conformal bootstrap II. c-minimization and precise critical exponents, J. Stat. Phys. **157**, 869 (2014).

[14] S. El-Showk, M. F. Paulos, D. Poland, S. Rychkov, D. Simmons-Duffin, and A. Vichi, Solving the 3D Ising model with the conformal bootstrap, Phys. Rev. D **86**, 025022 (2012).

[15] S. M. Chester, W. Landry, J. Liu, D. Poland, D. Simmons-Duffin, N. Su, and A. Vichi, Carving out OPE space and precise $O(2)$ model critical exponents, J. High Energy Phys. 06 (2020) 142.

[16] G. Fardelli, A. L. Fitzpatrick, and E. Katz, Constructing the infrared conformal generators on the fuzzy sphere, SciPost Phys. **18**, 086 (2024).

[17] R. Fan, Note on explicit construction of conformal generators on the fuzzy sphere, arXiv:2409.08257.

[18] H. W. J. Blöte, J. L. Cardy, and M. P. Nightingale, Conformal invariance, the central charge, and universal finite size amplitudes at criticality, Phys. Rev. Lett. **56**, 742 (1986).

[19] J. Cardy, Conformal invariance and statistical mechanics, in *Fields, Strings and Critical Phenomena*, edited by E. Brézin and J. Zinn-Justin, Les Houches, École d'Été de Physique Théorique Vol. 49 (North-Holland, Amsterdam, 1988), p. 169.

[20] J. L. Jacobsen and K. J. Wiese, Lattice realization of complex CFTs: Two-dimensional Potts model with $Q > 4$ states, Phys. Rev. Lett. **133**, 077101 (2024).

[21] A. B. Zomolodchikov, "Irreversibility" of the flux of the renormalization group in a 2D field theory, Pis'ma Zh. Eksp. Teor. Fiz. **43**, 565 (1986) [JETP Lett. **43**, 730 (1986)].

[22] S. Deser and A. Schwimmer, Geometric classification of conformal anomalies in arbitrary dimensions, Phys. Lett. B **309**, 279 (1993).

[23] M. J. Duff, Twenty years of the Weyl anomaly, Classical Quantum Gravity **11**, 1387 (1994).

[24] Z. Komargodski and A. Schwimmer, On renormalization group flows in four dimensions, J. High Energy Phys. 12 (2011) 099.

[25] J. L. Cardy, Is there a c-theorem in four dimensions? Phys. Lett. B **215**, 749 (1988).

[26] D. L. Jafferis, I. R. Klebanov, S. S. Pufu, and B. R. Safdi, Towards the F-theorem: $\mathcal{N} = 2$ field theories on the three-sphere, J. High Energy Phys. 06 (2011) 102.

[27] R. C. Myers and A. Sinha, Holographic c-theorems in arbitrary dimensions, J. High Energy Phys. 01 (2011) 125.

[28] D. L. Jafferis, The exact superconformal R-symmetry extremizes Z, J. High Energy Phys. 05 (2012) 159.

[29] I. R. Klebanov, S. S. Pufu, and B. R. Safdi, F-theorem without supersymmetry, J. High Energy Phys. 10 (2011) 038.

[30] M. P. Hertzberg and F. Wilczek, Some calculable contributions to entanglement entropy, Phys. Rev. Lett. **106**, 050404 (2011).

[31] H. Liu and M. Mezei, A refinement of entanglement entropy and the number of degrees of freedom, J. High Energy Phys. 04 (2013) 162.

[32] H. Casini and M. Huerta, Renormalization group running of the entanglement entropy of a circle, Phys. Rev. D **85**, 125016 (2012).

[33] L. Hu, W. Zhu, and Y.-C. He, Entropic F-function of 3D Ising conformal field theory via the fuzzy sphere regularization, Phys. Rev. B **111**, 155151 (2025).

[34] Z. Zhou, FuzzifiED: Julia package for numerics on the fuzzy sphere, arXiv:2503.00100.

[35] A. W. W. Ludwig and J. L. Cardy, Perturbative evaluation of the conformal anomaly at new critical points with applications to random systems, Nucl. Phys. B **285**, 687 (1987).

[36] M. Hogervorst, S. Rychkov, and B. C. van Rees, Truncated conformal space approach in d dimensions: A cheap alternative to lattice field theory? Phys. Rev. D **91**, 025005 (2015).

[37] A. M. Läuchli, L. Herviou, P. H. Wilhelm, and S. Rychkov, Exact diagonalization, matrix product states and conformal perturbation theory study of a 3D Ising fuzzy sphere model, SciPost Phys. **19**, 076 (2025).
[38] W. Zhu (private communication).
[39] S. Giombi and I. R. Klebanov, Interpolating between a and F, J. High Energy Phys. 03 (2015) 117.
[40] A. K. Hartmann, Calculation of partition functions by measuring component distributions, Phys. Rev. Lett. **94**, 050601 (2005).
[41] S. M. Chester and N. Su, Upper critical dimension of the 3-state Potts model, Phys. Rev. D **111**, L121701 (2025).
[42] https://docs.fuzzified.world/